Neutron reactions in the hohlraum at the LLNL National Ignition Facility

P. A. Bradley, G. P. Grim, A. C. Hayes, Gerard Jungman, R. S. Rundberg, J. B. Wilhelmy, and G. M. Hale
Los Alamos National Laboratory, Los Alamos, New Mexico 87545, USA

R. C. Korzekwa
Los Alamos National Laboratory, Los Alamos, New Mexico 87545, USA and
Department of Physics, University of Texas, Austin, Texas 78712, USA
(Received 27 January 2012; published 25 July 2012)

The National Ignition Facility (NIF) is designed to drive deuterium-tritium (DT) inertial confinement fusion targets to ignition using indirect radiation from laser energy captured in a hohlraum. The projected yields at NIF suggest that interactions of neutrons with the hohlraum can directly probe the neutron spectrum. Different physical parameters of the burning capsule can be probed by different neutron reactions. We suggest a variety of neutron reactions on the gold and uranium present in National Ignition Campaign hohlraums that will be useful for both neutron diagnostics and dosimetry at the NIF. The radiochemical daughter products may then be used to infer the neutron spectrum from the capsule. The downscattered neutrons may be studied by the (n,γ) and (n,n') reactions to infer the areal density of the capsule. The 14 MeV neutron fluence may be measured by $(n,2n)$ daughter products for comparison to neutron spectrometer data. The hydrodynamical mix in the capsule can be studied with RIF neutrons, which are probed by $(n,3n)$ reactions.

DOI: 10.1103/PhysRevC.86.014617 PACS number(s): 28.52.Cx, 82.80.Jp, 47.27.wj, 52.57.−z

I. INTRODUCTION

In indirect drive inertial confinement fusion the fuel capsule is placed inside a high-Z hohlraum. The hohlraum interior converts the laser energy into soft x rays that are used to ablate the outer surface of the capsule and thus compress the fuel. As of January 2012, the measured yields at NIF are close to 10^{15} neutrons, and the projected yields for ignited NIF capsules are up to 10^{18} neutrons. In both cases, the neutrons induce sufficient reactions in the hohlraum to use these 'incidental' reactions as diagnostics for thermonuclear burn in the capsule. The neutron fluence spectrum can be measured at NIF by time-of-flight (TOF) using a fast scintillator 12–20 m from the target [1]. Neutron activation [2] of other materials placed inside the chamber is also used to measure the 14 MeV yield, and in general, activation techniques can be used to probe the different energy components of the neutron spectrum. Neutron imaging [3] at NIF currently images both the 14 MeV neutrons and the 10–12 MeV neutrons. Neutrons above the 14 MeV peak can be produced by so-called reactions-in-flight, and the yield of these higher energy neutrons depends [4] on the details of the compressed capsule geometry and on plasma conditions. For these higher energy neutrons ($E_n \geqslant 22$ MeV) carbon activation through the $^{12}\mathrm{C}(n,2n)^{11}\mathrm{C}$ reaction in graphite disks placed inside the chamber has been proposed [5], and for sufficient yields the reaction-in-flight neutrons could also be imaged. Complementary to these techniques, reactions in the hohlraum can probe both high- and low-fluence components of the neutron spectrum because the hohlraum is within 10 mm of the deuterium-tritium (DT) capsule and almost the entire fluence passes through the hohlraum wall. The radiochemical daughter products from the gold and/or uranium in the hohlraum wall may then be used to infer the neutron spectrum form the capsule. The downscattered neutrons may be studied by the (n,γ) and (n,n') reactions to infer the areal density of the capsule. The 14 MeV neutron fluence may be measured by $(n,2n)$ daughter products for comparison to neutron spectrometer data. The hydrodynamical mix in the capsule can be studied with RIF neutrons, which are probed by $(n,3n)$ reactions. In principle, one can study dosimetry properties of additional elements besides Au and U by coating the hohlraum with the material of interest. Dosimetry data exist for Cr, Mo, Fe, Co, Ni, Cu, Zn, Y, Zr, Nb, Rh, Ag, Cd, I, La, Gd, Tm, Ta, W, and Th [6–10].

The NIF hohlraum is cylindrical in shape, and the design dimensions of the both the capsule and hohlraum depend to some extent on the input laser energy and the designed yield. Initial hohlraum designs were based on 1.8 MJ of laser energy. A second design was based on ignition attempts utilizing about 1 MJ of laser drive, while more recent designs have used observed NIF data to maximize laser-capsule coupling. Optimization of hohlraum energetics, laser propagation and absorption, laser conversion efficiency to x rays, and minimization of x-ray losses in the wall and laser entrance hole (LEH) dictate the materials used for the wall and windows. In going from one hohlraum design to another the dimensions of the hohlraum change, but this only affects the results of neutron-hohlraum reactions by an overall scaling factor proportional to the ratio of the old and new hohlraum design areas. In the present calculations we concentrate on a 1 MJ laser-energy capsule-hohlraum design [11] for which the hohlraum dimensions are 9.22 mm long and 5.1 mm in diameter, with LEHs at each end of the cylinder (see Fig. 1). The design [11] considered here involves an inner gold layer about 0.2 μm thick on a 30 μm (or thicker) gold or uranium (gold/uranium "cocktails" have also been proposed) wall. The LEH are 50% of the diameter of the cylinder, and are made of polyamide. We examine the sensitivity of

the neutron interactions with these hohlraum materials to the detailed shape of the neutron fluence, and hence to the physics characterizing the burning DT gas. Our emphasis is on reactions that have decay signatures, but measuring isotopes with mass spectroscopy is also possible and could provide important supplementary information.

The physics of the implosion and burn of the capsule is described using a one-dimensional (1-D) hydrodynamics code. The code allows for hydrodynamical mixing of material across different layers of the capsule. However, by its 1-D nature, it cannot describe asymmetric or other 2-D or 3-D imperfections in the implosions. Thus, even for large mixing scenarios, the predicted yields are considerably higher than current NIF yields. Nonetheless, the calculations provide useful information on the general trends expected in the change of the shape of the neutron fluence as the capsule performance varies over two orders of magnitude, 6×10^{16}–5×10^{18} neutrons. These changes may prove useful in analyzing actual hohlraum data from NIF shots.

II. CAPSULE AND MIX MODELING

The capsule design used in this work represents a typical DT-fueled ignition design. It uses a layer of frozen DT approximately 90 μm thick $\rho = 0.25$ g $\cdot$ cm^{-3} with an inner radius of 725 μm and an outer radius of 825 μm. Inside the layer of DT ice is a sphere of DT gas with gas fill $\rho = 0.0005$ g $\cdot$ cm^{-3}. Surrounding the DT ice is a shell (inner radius 825 μm and outer radius 1000 μm) made of either ^{9}Be (doped with $<$1% Cu) or plastic. In the present work we assume a Be(0.3%Cu) shell in modeling the capsule implosion and burn, but our results pertaining to neutron interactions in the hohlraum hold equally well for plastic or other shells capable of achieving similar yields.

The calculations were carried out using a one-dimensional hydrodynamical burn code. With a hohlraum temperature of $\sim$300 eV (requiring a total laser energy of 1 MJ), the capsule is predicted to reach a peak $\langle \rho R \rangle_{DT} \sim 1.2$ g $\cdot$ cm^{-2} and to achieve ignition with a thermonuclear yield of 16.65 MJ. This latter yield is predicted in calculations in which no mixing occurs between the shell material and the DT fuel. However, during the implosion phase, hydrodynamic instabilities at the interface between the shell and fuel can occur and these result in shell/fuel mixing which degrades the yield. The mixing can be parameterized in terms of a mixing length which approximates the distance that the shell material mixes into the DT fuel, and in the present calculations this mixing length is treated as an unknown parameter. To model the hydrodynamical mix we used the Scannapieco and Cheng model [12] which allows a fully dynamical treatment of the problem. In this model the mixing length is expressed in terms of the difference of the velocities of the two species involved in the mix and is parametrized by a single dimensionless input variable α as

$$L_{\rm mix}(t) = \alpha \int_0^t \left(\frac{\rho(\tau)}{\rho(t)}\right)^{\beta} |U(r,t)_{DT} - U(r,t)_{\rm shell}| d\tau, \quad (1)$$

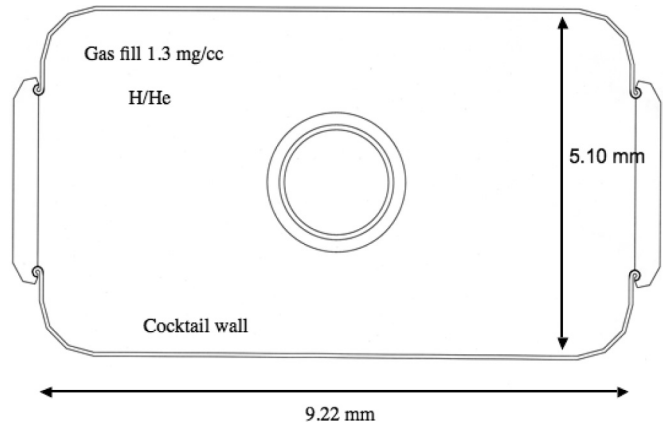

FIG. 1. Schematic of a 1 MJ laser-heated hohlraum design. The cylindrical hohlraum is fabricated from Au or U, although other materials or composites with similar opacities are possible. The wall thickness is at least 30 μm. The polyamide laser entrance holes at each end of the cylinder are 2.54 mm in diameter. The hohlraum is filled with 50/50 1.3 mg/cc H/He gas. The nominal capsule design involves a 0.3 atom% Cu doped Be shell of inner radius 825 μm and outer radius 1000 μmm surrounding a layer of DT ice and DT gas. The DT ice layer has an inner radius of 735 μm and an outer radius of 825 μm.

where $U(r,t)_i$ are the time and spatially dependent velocities of the fuel and shell material and the term $(\rho(\tau)/\rho(t))^{\beta}$ adjusts for density changes during compression or expansion of the mixing layer. For spherical implosions $\beta = 1/3$.

Analyses [13] of inertial confinement fusion experiments at the NOVA and OMEGA Laser facilities using the same mix model suggest $\alpha \simeq 0.06$. The capsules considered in the NOVA and OMEGA studies contained two material phases, the ablator material and the DT gas. For NIF capsules there are three material phases, namely, the ablator material, the DT ice and the DT gas. Though there is no *a priori* reason to expect that the mixing parameter between the ablator and ice and that between the ice and gas are the same, we nonetheless used a single mixing parameter for the two interfaces. The reasonable range expected [12] for the parameter α is $\alpha \sim 0.0$–0.13 and we examined several mixing scenarios in this range, namely, $\alpha = 0.0, 0.01, 0.03, 0.06, 0.11, 0.13, 0.16$. We note that at the upper end of this range ($\alpha = 0.16$) the mixing is significant enough to cause ignition failure.

As mixing at the shell-ice and simultaneously the ice-gas interfaces (shell-ice-gas mixing) increases, the yield progressively decreases, going from 6.1×10^{18} to 4.9×10^{16} DT reactions as α goes from 0.0 to 0.16, respectively. In addition to degrading the yield, the mixing significantly changes other conditions of the plasma. In particular, the peak fuel average temperature decreases from $\sim$32 keV for the fully ignited capsule to 5 keV for the failed capsule. The density at the inner most part of the ice generally increases with mixing because the corresponding lower temperatures in the fuel allow the capsule to compress more, and, for example, the density for the failed capsule is $\sim$300% higher than that of the ignited capsule. These systematic trends are consistent with the mixing analyses [13] of experiments from NOVA and OMEGA.

III. THE NEUTRON FLUENCE

The vast majority of neutrons are produced during the burn by the $d(t,n)\alpha$ reaction with energies $E_n = 14.1$ MeV and the neutron spectrum is dominated by a peak at this energy, Fig. 2. The width of the peak is determined by the temperature of the DT burn. In addition to the primary 14 MeV peak, there are significant contributions from both low-energy and high-energy reaction-in-flight (RIF) neutrons. The low-energy part of the spectrum is dominated by down scattering of the 14 MeV neutrons due to inelastic scattering or $(n,2n)$ reactions on the D or T ions. There are additional low-energy contributions from $d+d$ reactions and $t+t$ reactions. At energies above the thermally broadened 14 MeV peak, the spectrum is dominated (>75% chance) by RIF neutrons that are created when a neutron knocks a D or T ion to high energy and a subsequent DT reaction-in-flight produces a neutron with energy up to 30 MeV. The low-energy spectrum (below the thermally broadened 14 MeV peak) represents roughly 12% of the total neutron fluence, whereas the RIF neutrons represent less than 0.3%.

A. Down-scattered neutrons and $\langle \rho r \rangle$

The mean-free path for neutrons in the capsule is sufficiently long that on average a neutron has only about a 10% chance of scattering before escaping the capsule. Thus, the low-energy neutron spectrum can be approximated by a single scattering model and the down-scattered neutrons are a direct measure of the areal density $\langle \rho r \rangle$ in the capsule [14,15]. As the hydrodynamic mix between the shell and the DT fuel increases, the ρr also increases and the relative number of low-energy neutrons increases. This can be seen in Fig. 3, where we graph the neutron fluence spectra per unit yield for each value of the mixing parameter. The down-scattered neutron spectrum rises steadily above about 6 MeV. This is primarily due to the differential cross section for scattering of 14.1 MeV neutrons from D or T ions. At lower energies primary and down-scattered $d+d$ and $t+t$ neutrons become important. We note that the fraction of the low-energy neutrons arising from the $d+d$ and $t+t$ reactions is temperature dependent and extracting information on $\langle \rho r \rangle$ from the measured low-energy spectrum requires corrections for these contributions.

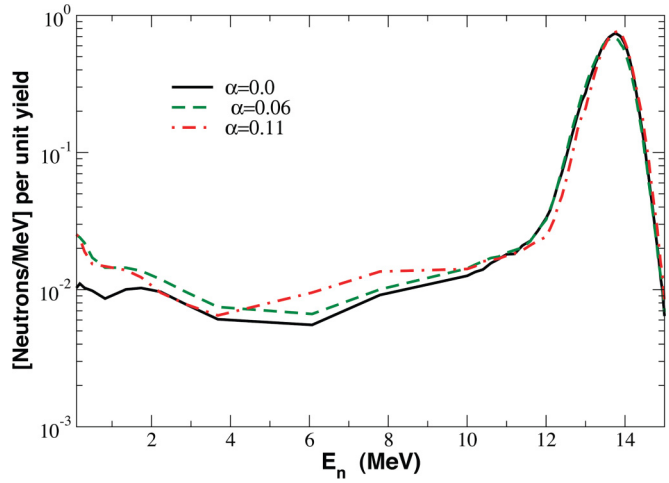

FIG. 3. (Color online) The low-energy neutron spectra for three different yields obtained by varying the mix parameter (α). The spectra have been normalized and integrated to unity. As hydrodynamical mix between the shell and DT fuel increases, ρr increases and the fraction of low-energy neutrons also increases.

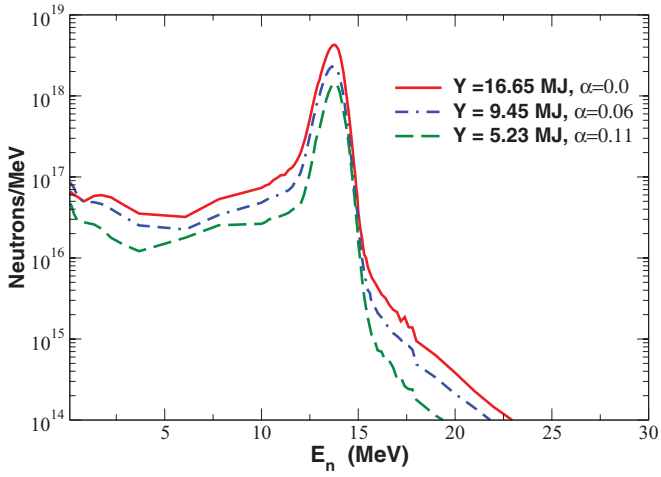

FIG. 2. (Color online) Neutron spectra for three different yields obtained by varying the mix parameter (α) in the Scannapieco and Cheng model. About 12% of the fluence lies at energies below the thermally broadened 14.1 MeV peak and less than 0.3% corresponds to the high-energy RIF neutrons.

There are two neutron reactions on the hohlraum materials that probe the low-energy part of the spectrum, namely, radiative neutron capture and inelastic neutron scattering. The latter is detectable only when it leads to an isomeric state of the nucleus. ^{197}Au has a 7.8 sec isomer at 409 keV, which decays 73% of the time via a 280 keV γ ray, which could be detected by prompt radiochemical techniques. If a gold/uranium cocktail hohlraum were used, it could hinder the measurement of this γ ray because of the large γ-ray background produced on the same time scale by the decay of the fission products from fission induced in ^{238}U by the 14 MeV neutrons. Another problem is the requirement for an in situ counting system or rapid transport of the radioactive samples to an external gamma-ray counter. For the sake of discussion, in the rest of this section we will ignore the radiation background from uranium fission and examine the isomer of ^{197}Au as a monitor of the neutron fluence.

The (n,n') cross section to the isomer of ^{197}Au is shown in Fig. 4. The cross section shows a broad peak from about 2–9 MeV, with a tail extending to high energies. Because of this tail the average neutron energy probed ($\overline{E} \equiv \langle \sigma(E)\phi(E) \rangle / \langle \phi(E) \rangle$) is about 10 MeV, and about 50% of the reactions are induced by the thermally broadened 14 MeV peak. The expected number of reactions scales with the neutron yield and is 5×10^{13} for a 16.65 MJ yield. As discussed below, to extract information solely on the low-energy neutrons requires an analysis involving subtraction of the 14 MeV neutron contribution. When this correction is

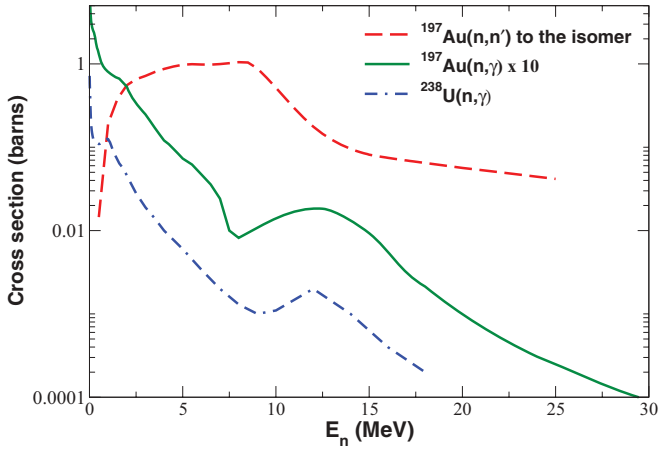

FIG. 4. (Color online) The (n,γ) cross sections for ^{197}Au and ^{238}U and the (n,n') cross section s to the 7.8 sec, 409 keV isomer of ^{197}Au.

made, we expect 2.6×10^{13} (n,n') reactions to the isomer of ^{197}Au from low-energy neutrons.

The capture reactions on both ^{197}Au and ^{238}U probe considerably lower-energy ($\overline{E} \sim 3.5$ MeV) neutrons than the (n,n') reaction. In the case of ^{197}Au, the half-life of the daughter nucleus ^{198}Au is 2.7 d, which β-decays to ^{198}Hg resulting in a 400 keV β-delayed γ ray 100% of the time. In the case of ^{238}U, the 23.47 min β decay of ^{239}U leads to a 74.7 keV γ ray in ^{239}Np. We expect about 1.4×10^{12} (n,γ) reactions on Au and 2.7×10^{12} on U as shown in Table I. We note that the 2.27 day isomer of ^{198}Au, which can be populated in the (n,γ) reaction, decays by internal conversion to the ground state emitting a strong 204 keV γ ray. This may have to be corrected for in any data analysis, but this correction is straight forward.

As can be seen in Fig. 4, the neutron capture cross section drops off steadily with neutron energy until one reaches sufficiently high energies ($E_n \sim$ 12–14 MeV), corresponding

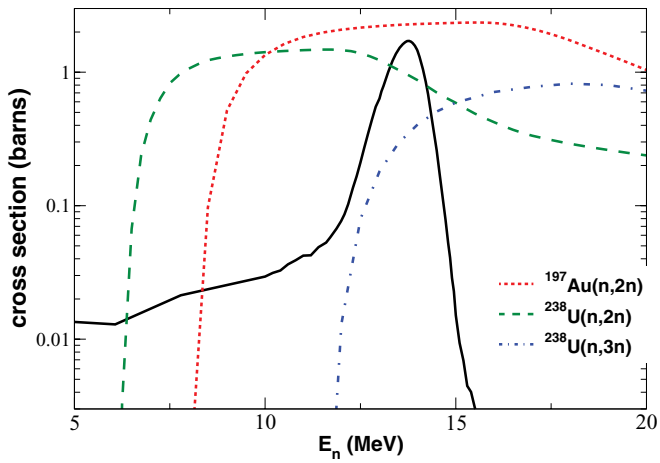

FIG. 5. (Color online) Reactions probing the thermally broadened 14 MeV peak (black line). The neutron spectrum is included only for visual aid purposes and the scale presented in the figure does not apply to it.

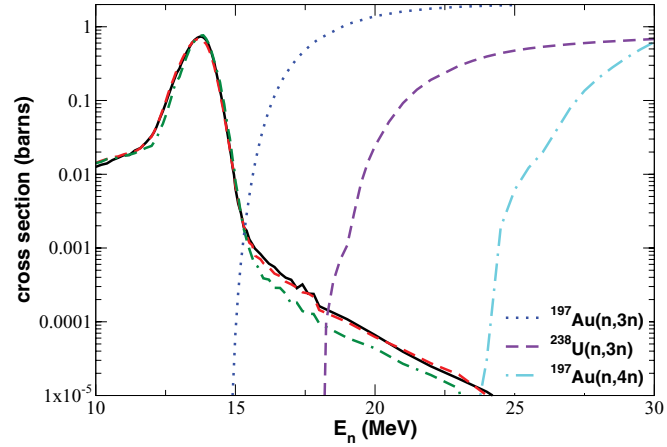

FIG. 6. (Color online) Reactions probing the RIF neutrons. The spectra for the three mixing scenarios are normalized to integrate to unity. The solid (black) curve is the no-mix case, the dashed (red) curve $\alpha = 0.06$, and the dashed-dot (green) curve $\alpha = 0.11$.

to the energy of the giant dipole resonance, where so-called direct-semidirect (DSD) processes start to contribute to the cross section. At these energies the cross sections for both Au and U show a resonance and increase to about ∼1 mb. As discussed below, a correction needs to be made for these DSD contributions in order to extract the low-energy neutron fluence from neutron capture measurements. An additional concern is that low-energy neutrons produced by scattering with the hohlraum could induce an additional (and potentially large) background contribution to the total number of capture reactions taking place.

B. The 14 MeV fluence

Radiochemical techniques can be used to monitor the 14 MeV fluence in the capsule [16] using the $(n,2n)$ reactions on the Cu in the Be shell, although backgrounds from other sources of copper associated with the hohlraum need to be taken into account. Areas of concern include the mounting equipment for the hohlraum cryogenics and the cooling rings.

Here we examine the $(n,2n)$ [and $(n,3n)$] reactions on the gold and uranium [17] in the hohlraum which provide an alternate probe for the 14 MeV peak. We can use the measured neutron yield and $(n,2n)$ reaction products or gold and uranium to better constrain the $(n,3n)$ reactions. The neutron threshold for the $(n,2n)$ reaction differs for each nucleus and a comparison between integral $(n,2n)$ measurements provides a measure of the neutron down-scattering from 14 MeV to threshold, which in turn is a measure of $\langle \rho r \rangle$. However, the dominant contribution to the $(n,2n)$ reactions for a NIF spectrum is always from the 14 MeV peak.

For the 16.65 MJ capsule, we expect 6×10^{14} $(n,2n)$ reactions on ^{197}Au as shown in Table I. The decay of ^{196}Au results (87%) in a 356 keV γ ray. Assuming a 1% detection efficiency, this would provide an easily detectable signal. In the case of ^{238}U$(n,2n)$, 7×10^{14} reactions are predicted and a 208 keV γ ray emitted in the 6.75 d decay of ^{237}U also provides a strong signal for 1% detection efficiency.

TABLE I. Gold and uranium reactions in the hohlraum.

Reaction	Threshold (MeV)	$\overline{E}$[a] (MeV)	Half-life of product	Reactions for 16.65 MJ capsule
Low-energy reactions:				
^{197}Au$(n,\gamma)^{198}$Au	–	3.5	2.7 d	1.4×10^{12}
^{238}U$(n,\gamma)^{239}$U	–	3.0		2.7×10^{12}
^{197}Au$(n,n')^{197}$Au^m	0.4	10.7	7.8 sec	5.4×10^{13}
14 MeV reactions:				
^{197}Au$(n,2n)^{196}$Au	8.1	13.5	6.2 d	6.2×10^{14}
^{197}Au$(n,2n)^{196}$Au^m			9.6 hr	
^{238}U$(n,2n)^{237}$U	6.18	13.2	6.75 d	7.8×10^{14}
^{238}U$(n,3n)^{236}$U	11.6	13.9	2.3×10^7 yr	2.2×10^{14}
RIF reactions:				
^{197}Au$(n,3n)^{195}$Au	14.79	19.7	186 d	1.7×10^{11}
^{197}Au$(n,4n)^{194}$Au	23.2	27.4	38 hr	1.0×10^8
^{238}U$(n,4n)^{235}$U	18.0	23.0	stable	2×10^{10}
Fission:				
^{238}U$(n$,fission$)$	~ 1	13.2		8.3×10^{14}

[a] $\overline{E} \equiv \langle \sigma(E)\phi(E) \rangle / \langle \phi(E) \rangle$. We note that the ^{238}U$(n, 4n)^{235}$U reaction is unlikely to be measurable because the ^{235}U present in depleted uranium would overwhelm the signal.

The average neutron energies probed by the $(n,2n)$ reaction for gold and uranium are 13.5 MeV and 13.2 MeV, respectively. The thresholds for the reactions are significantly lower than 14 MeV (see Fig. 5), but because of the very large suppression of the low-energy fluence these reactions provide a clean monitor of the 14 MeV fluence. The ^{238}U$(n,3n)^{236}$U reaction [17] also probes the 14 MeV fluence cleanly, but the very long half-life of ^{236}U would require other detection techniques, perhaps mass spectroscopy.

C. Reaction-in-flight neutrons (RIFs)

The collision of a D or T ion with a high energy neutron causes that ion to depart from the thermal distribution; it may then react in flight with another ion while its kinetic energy is much higher than ions in the thermal distribution. If such a DT reaction occurs, the resultant neutron energy can be considerably higher than 14 MeV. Superthermal ions can also result from ion-ion collisions. However, the dominant scenario for producing RIF neutrons is the energetic DT reactions of the first scenario above. We note that the exact number of RIF reaction products produced also depends on the D,T stopping power [18].

The RIF neutrons can be detected by observing the reaction products of ^{197}Au$(n,3n)^{195}$Au. The threshold for this reaction is 14.79 MeV and neutrons from the thermal broadening of the 14 MeV peak contribute essentially nothing to the total $(n,3n)$ reaction yield (see Fig. 6). Thus, the ^{197}Au$(n,3n)$ reaction probes the full energy range of the RIF spectrum compared to the carbon activation method [^{12}C$(n,2n)$] for which the threshold is 18.7 MeV. The average neutron energy probed by this reaction is $\overline{E} \sim 19.7$ MeV. For our 16.65 MJ capsule we expect 1.7×10^{11} reactions (see Table I). The product nucleus ^{195}Au has a half-life of 186 d and emits several γ rays in the 50–100 keV range. The long half-life means that a measurement can be made after most other radioactive nuclides in the debris have decayed, and observation of the ^{195}Au decay may be possible at a low background facility such as the Waste Isolation Pilot Plant (WIPP) facility in Carlsbad, New Mexico.

A probe of the higher energy component of the RIF neutron spectrum is the ^{197}Au$(n,4n)^{194}$Au reaction, which has a threshold of 23.2 MeV (see Fig. 6). For our high-yield capsule we expect 1×10^8 reactions. The half-life of ^{194}Au is 38 hr and it decays with a 1.6% branch by β^+ decay emitting a (2.1%) 1.92 MeV and a (3.8%) 2.03 MeV γ ray. This measurement may be feasible using a thin layer of Pb to shield lower-energy γ rays.

The ^{238}U$(n,4n)$ reaction [17] has a threshold of 18 MeV (see Fig. 6) and is similar to the ^{12}C$(n,2n)$ reaction. We expect to produce about 10^{10} stable ^{235}U atoms (see Table I). However, the ^{238}U$(n, 4n)^{235}$U reaction is unlikely to be measurable because the ^{235}U present in depleted uranium would overwhelm the signal.

The number of RIF neutrons drops significantly with the degree of mix in the capsule [4] and the expected number of reactions for the ^{197}Au $(n,4n)$ reaction drops to 2.8×10^7 and the $(n,3n)$ reaction to 3.4×10^{10} for the 5.23 MJ capsule. Thus, for sufficiently low capsule yields the signal for RIF neutrons eventually becomes difficult to detect except at a very low background facility such as WIPP.

IV. CORRECTIONS TO THE LOW-ENERGY AND RIF SIGNALS FROM THE 14 MEV PEAK

Radiochemistry provides an integral measure of the neutron spectrum over an energy dependent cross section. To determine the neutron fluence in a subenergy interval (the low-energy or RIF region) a correction needs to be made to subtract contributions from neutrons outside the interval of interest. In both cases these corrections arise from the contributions

TABLE II. Correction to reactions probing low-energy and RIF neutrons obtained by subtracting the contribution from the 14 MeV peak. We note that for the RIF neutrons essentially no correction is needed. $\overline{E}$ and Corrected $\overline{E}$ are the average neutron energies probed by the reaction when the 14 MeV peak is and is not included, respectively.

Reaction	$\overline{E}$ (MeV)	Corrected $\overline{E}$ (MeV)	Full spectrum	Peak subtracted
Low-energy reactions:				
^{197}Au$(n,\gamma)^{198}$Au				
16.65 MJ	5.06	1.62	1.41×10^{12}	1.01×10^{12}
9.45 MJ	3.43	1.17	1.24×10^{12}	1.01×10^{12}
5.23 MJ	3.42	1.18	6.69×10^{11}	5.49×10^{11}
^{197}Au$(n,n')^{197}$Au^{m}				
16.65 MJ	10.68	7.21	5.40×10^{13}	2.43×10^{13}
9.45 MJ	10.28	6.95	3.26×10^{13}	1.60×10^{13}
5.23 MJ	10.18	7.15	1.85×10^{13}	9.83×10^{12}
^{238}U$(n,\gamma)^{239}$U				
16.65 MJ	4.41	1.55	2.66×10^{12}	2.03×10^{12}
9.45 MJ	3.09	1.21	2.30×10^{12}	1.95×10^{12}
5.23 MJ	3.11	1.21	1.22×10^{12}	1.04×10^{12}
^{197}Au$(n,3n)^{195}$Au				
16.65 MJ	1.97	1.97	1.73×10^{11}	1.73×10^{11}
9.45 MJ	1.98	1.98	9.38×10^{10}	9.38×10^{10}
5.23 MJ	2.00	2.00	3.41×10^{10}	3.41×10^{10}

from the thermally broadened 14 MeV peak. In Table II we list the change in the number of reactions obtained when the contributions from the 14 MeV peak are subtracted for each of the neutron spectra displayed in Fig. 2. The largest corrections occur for the (n,γ) and (n,n') reactions, where the 14 MeV peak contributes 20–50 % of the total reaction yield. The correction for the ^{197}Au$(n,3n)$ reaction is negligible, and this $(n,3n)$ reaction acts as a clean probe of the RIF neutrons.

There is an additional complication arising from the temperature dependence of the peak contribution to these reaction yields. To examine this we define a distribution function for outgoing neutron laboratory energies,

$$f(E_n) = \frac{\phi}{\langle \sigma v \rangle} \frac{d\langle \sigma v \rangle}{dE_n}, \tag{2}$$

in which $\langle \sigma v \rangle$ is the usual Maxwellian-averaged nuclear reaction rate for a given temperature. The expression for this quantity is somewhat complicated [19], but in the case that the Q-value for the reaction is much larger than the temperature T, it can be approximated as

$$f(E_n) \approx \frac{\phi M}{\sqrt{4\pi Q T m_n m_r}} \left[\exp\left(\frac{-(\sqrt{M E_n} - \sqrt{m_r Q})^2}{m_n T} \right) \right], \tag{3}$$

with m_n the mass of the neutron and m_r the mass of the residual particle in the final state, and $M = m_n + m_r$.

We examined the temperature dependence, of the contributions to the various reactions and found very little T dependence. The exception was the ^{197}Au$(n,3n)$ reaction, where the threshold for the reaction is at 14.79 MeV. However, despite this strong dependence the contribution of the 14.1 peak to the ^{197}Au$(n,3n)$ reaction remained negligibly small for temperatures $\sim$ 10–100 keV.

TABLE III. Reaction yields as a ratio to the ^{197}Au$(n,2n)$ yield for three different mixing parameters (α). As the ρr increases the relative number of low-energy reactions increases. This is not the case for the RIF reactions, where the trend is in the opposite direction.

Reaction	Ratio to the number of ^{197}Au$(n,2n)$ Reactions		
	$\alpha = 0$	$\alpha = 0.06$	$\alpha = 0.11$
Low-energy reactions:			
^{197}Au$(n,\gamma)^{198}$Au	1.64×10^{-3}	2.96×10^{-3}	2.92×10^{-3}
^{197}Au$(n,n')^{197}$Au^{m}	3.95×10^{-2}	4.69×10^{-2}	5.23×10^{-2}
^{238}U$(n,\gamma)^{239}$U	3.3×10^{-3}	5.71×10^{-3}	5.53×10^{-3}
RIF reactions:			
^{197}Au$(n,3n)^{195}$Au	2.81×10^{-4}	2.75×10^{-4}	1.81×10^{-4}
^{197}Au$(n,4n)^{194}$Au	1.72×0^{-7}	1.45×10^{-7}	1.47×10^{-7}
^{238}U$(n,4n)^{235}$U	3.31×10^{-5}	3.41×10^{-5}	2.53×10^{-5}

Finally, we examine the sensitivity of the (n,γ) and $(n,3n)$ (RIF) reactions to variations in the mixing parameter (and hence ρr), as shown in Table III. The number of (n,γ) reactions increases with ρr (and α), because there are more downscattered neutrons with increasing ρr and this implies more reactions on Au or U due to the increasing (n,γ) cross section as the neutron energy decreases. By contrast, the number of number of RIF reactions decreases with increasing ρr, because the burn temperature is decreasing, which decreases the number of high energy neutrons necessary for RIF reactions.

V. SUMMARY AND CONCLUSIONS

Radiochemical techniques offer a novel method of measuring the details of the neutron spectra from NIF capsules. We find that the neutron-induced reactions in the hohlraum could help to map out the three main regions of the spectrum, namely, the low-energy, the thermally broadened 14 MeV, and the RIF neutrons. In this paper we have mainly addressed techniques utilizing a gold/uranium hohlraum for generality. We summarize our results in Table III, where we present the reaction yields from various capture and RIF reactions as ratios to the reference ^{197}Au$(n,2n)$ reaction. The ability to add new materials to the hohlraum, behind the cocktail layer, opens the possibility for new classes of measurements. The use of more high energy threshold detector materials would allow a more detailed analysis of the the RIF neutrons which may place additional constraints on the mix over the proposed β-mix method [20]. The present work suggests that radiochemistry is likely to be an important diagnostic for neutron production at the NIF.

[1] G. J. Schmid, R. L. Griffith, N. Izumi, J. A. Koch, R. A. Lerche, M. J. Moran, T. W. Phillips, R. E. Turner, V. Yu. Glebov, T. C. Sangster, and C. Stoeckl, Rev. Sci. Instrum. **74**, 1828 (2003).

[2] G. W. Cooper and C. L. Ruiz, Rev. Sci. Instrum. **72**, 814 (2001).

[3] G. P. Grim, G. L. Morgan, M. D. Wilke, P. L. Gobby, C. R. Christensen, D. C. Wilson *et al.*, Rev. Sci. Instrum. **75**, 3572 (2009), and references therein.

[4] A. C. Hayes, P. A. Bradley, G. P. Grim, G. Jungman, and J. B. Wilhelmy, Phys. Plasmas **17**, 012705 (2010).

[5] V. Yu. Glebov, C. Stoeckl, T. C. Sangster, D. D. Meyerhofer, and P. B. Radha, Rev. Sci. Instrum. **74**, 1717 (2003).

[6] O. Bersillon, L. R. Greenwood, P. J. Griffin, W. Mannhart, H. J. Nolthenius, R. Paviotti-Corcuera, K. I. Zolotarev, E. M. Zsolnay, P. K. McLaughlin, and A. Trkov, "International Reactor Dosimetry File 2002 (IRDF-2002)," Technical Report Series No. 452, International Atomic Energy Agency, Vienna, Austria, December (2006).

[7] L. R. Greenwood and A. L. Nichols, "Review the Requirements to Improve and Extend the IRDF Library (International Reactor Dosimetry File (IRDF-2002))," TINDC(NDS)-0507, International Atomic Energy Agency, Vienna, Austria, January (2007).

[8] K. I. Zolotarev, "Re-evaluation of Microscopic and Integral Cross-Section Data Important Dosimetry Reactions," INDC(NDS)-0526, International Atomic Energy Agency, Vienna, Austria, August (2008).

[9] K. I. Zolotarev, "Re-evaluation of Cross-Section Data from Threshold to 40-60 MeV for Specific Nuclear Reactions Important for Neutron Dosimetry Applications", INDC(NDS)-0546, International Atomic Energy Agency, Vienna, Austria, April (2009).

[10] K. I. Zolotarev, "Evaluation of Cross-Section from Threshold to 40 MeV for Some Neutron Reactions Important for Fusion Dosimetry Applications", INDC(NDS)-0584, International Atomic Energy Agency, Vienna, Austria, November (2010).

[11] P. A. Bradley and D. C. Wilson, Internal Los Alamos Report No. LA-UR-06-3288.

[12] A. J. Scannapieco and B. L. Cheng, Phys. Lett. A **299**, 49 (2002).

[13] D. C. Wilson, A. J. Scannapieco, C. W. Cranfill, M. R. Clover, and N. M. Hoffman, Phys. Plasmas **10**, 4427 (2003).

[14] D. C. Wilson, W. C. Mead, L. Disdie, M. Houry, J.-L. Bourgade, and T. J. Murphy, Nucl. Instrum. Methods Phys. Res. A **488**, 400 (2002).

[15] H. Azechi, M. D. Cable, and R. O. Stapf, Laser Part. Beams **9**, 119 (1991).

[16] M. C. Miller, J. R. Celeste, M. A. Stoyer, J. Suter, M. T. Tobin, J. Grun, J. F. Davis, C. W. Barnes, and D. C. Wilson, Rev. Sci. Instrum. **72**, 537 (2002).

[17] M. B. Chadwick, M. Herman, P. Oblozinsky, M. E. Dunn, Y. Danon, A. C. Kahler, D. L. Smith, B. Pritychenko *et al.*, Nucl. Data Sheets **112**, 2887 (2011); see also P. G. Young, M. B. Chadwick, R. E. MacFarlane, P. Talou, T. Kawano, D. G. Madland, W. B. Wilson, and C. W. Wilkerson, *ibid.* **108**, 2589 (2007) (see pp. 2626–2627 especially).

[18] R. L. Singleton, Phys. Plasmas **15**, 056302 (2008).

[19] G. M. Hale (unpublished).

[20] A. C. Hayes, G. Jungman, J. C. Solem, P. A. Bradley, and R. S. Rundberg, Mod. Phys. Lett. **21**, 1029 (2006).